Theor Chem Account (2008) 119:319–327
DOI 10.1007/s00214-007-0387-2

REGULAR ARTICLE

Theoretical studies on the reactions of hydroxyl radicals with trimethylsilane and tetramethylsilane

Hui Zhang · Gui-Ling Zhang · Ying Wang · Xiao-Yang Yu · Bo Liu · Jing-Yao Liu · Ze-Sheng Li

Received: 20 March 2007 / Accepted: 27 August 2007 / Published online: 5 October 2007

Abstract The multiple-channel reactions OH + SiH$(CH_3)_3$ → products (R1) and the single-channel reaction OH + $Si(CH_3)_4$ → $Si(CH_3)_3CH_2 + H_2O$ (R2) have been studied by means of the direct dynamics method at the BMC-CCSD//MP2/6-311+G(2d,2p) level. The optimized geometries, frequencies and minimum energy path are all obtained at the MP2/6-311+G(2d,2p) levels, and energy information is further refined by the BMC-CCSD (single-point) level. The rate constants for every reaction channels are calculated by canonical variational transition states theory (CVT) with small-curvature tunneling (SCT) contributions over the temperature range 200–2,000 K. The theoretical total rate constants are in good agreement with the available experimental data, and the three-parameter expression $k_1 = 2.53 \times 10^{-21} T^{3.14} \exp(1,352.86/T)$, $k_2 = 6.00 \times 10^{-19} T^{2.54} \exp(-106.11/T)$ (in unit of cm^3 $molecule^{-1}s^{-1}$) over the temperature range 200–2,000 K are given. Our calculations indicate that at the low temperature range, for reaction R1, H-abstraction is favored for the SiH group, while the abstraction from the CH_3 group is a minor channel.

Electronic supplementary material The online version of this article (doi:10.1007/s00214-007-0387-2) contains supplementary material, which is available to authorized users.

H. Zhang · G.-L. Zhang · X.-Y. Yu · B. Liu (✉)
College of Chemical and Environmental Engineering, Harbin University of Science and Technology, Harbin 150080, People's Republic of China
e-mail: hust_zhanghui1@hotmail.com

Y. Wang · J.-Y. Liu · Z.-S. Li
Institute of Theoretical Chemistry, State Key Laboratory of Theoretical and Computational Chemistry, Jilin University, Changchun 130023, People's Republic of China

1 Introduction

Silane and its methyl-substituted homolog are considered as important reagents in plasma chemical vapor deposition (CVD) and in the semiconductor manufacturing process. Tetramethylsilane is frequently used as a solvent. The use of volatile silicon compounds may lead to their emission into the atmosphere, where they can be removed by reactions with a variety of reactive species, such as hydroxyl and nitrate radicals. For most hydrocarbons, hydrogen abstraction by OH radicals is one of the major channels for their removal in the atmosphere [1,2]. For reaction $SiH(CH_3)_3$ + OH, the hydrogen atom can be abstracted from SiH group and CH_3 group, as a result, two reaction pathways are feasible, denoted as R1a and R1b, respectively. For the reaction $Si(CH_3)_4$ + OH, there exists only one hydrogen abstraction channel, that is, H-abstraction from the CH_3 group denoted as R2 as follows:

$$OH + SiH(CH_3)_3 \rightarrow Si(CH_3)_3 + H_2O \quad \text{(R1a)}$$

$$\rightarrow SiH(CH_3)_2CH_2 + H_2O \quad \text{(R1b)}$$

$$OH + Si(CH_3)_4 \rightarrow Si(CH_3)_3CH_2 + H_2O \quad \text{(R2)}$$

With the flash-photolysis resonance-fluorescence (FP-RF) technique, the overall rate constants of the title reactions have been investigated by Goumri et al. [3], and the rate constants they measured were represented by the expression $k_1 = (3.1 \pm 0.4) \times 10^{-11}$ cm^3 $molecule^{-1}s^{-1}$ at 293–297 K for the OH + $SiH(CH_3)_3$ reaction and $k_2 = (1.2 \pm 0.2) \times 10^{-12}$ cm^3 $molecule^{-1}s^{-1}$ at 293–297 K for the

$OH + Si(CH_3)_4$ reaction. For the $OH + Si(CH_3)_4$ reaction, the rate constants obtained by Atkinson et al. [4] at 297 ± 2 K, by Sommerlade et al. [5] at 297 ± 2 K, and by Tuazon et al. [6] at 298 ± 2 K were $(1.00 \pm 0.27) \times 10^{-12}$, $(1.28 \pm 0.46) \times 10^{-12}$, and $(8.5 \pm 0.9) \times 10^{-13}$ (in unit of $cm^3 mol^{-1} s^{-1}$), respectively. The k_2 value of reaction R2 taken from Goumri et al.'s work [3] is in good agreement with those given by Atkinson et al. [4], Sommerlade et al. [5], and Tuazon et al. [6] at room temperature. To the best of our knowledge, the rate constants of the title reactions have not been studied theoretically.

In this work, dual-level direct dynamics method [7–10] is employed to study the kinetics of OH radical reactions with $SiH(CH_3)_3$ and $Si(CH_3)_4$. The potential energy surface information, including geometries, energies, gradients, and force constants of all the stationary points (reactants, hydrogen-bonded complexes (HBC), products, and saddle points), and some extra points along with the minimum energy path (MEP) are obtained directly from electronic structure calculations. Single-point energies are calculated at the BMC-CCSD level [11]. Subsequently, by means of the POLYRATE 9.1 program [12], the rate constants of these reaction channels are calculated by the variational transition states theory (VTST) [13,14] proposed by Truhlar and his co-workers. The comparison between the theoretical and experimental results is discussed. Our results may be helpful for further experimental investigations.

2 Computational method

In the present work, the equilibrium geometries and frequencies of all the stationary points (reactants, HBC, products, and saddle points) are optimized at the restricted or unrestricted second-order Møller–Plesset perturbation (MP2) [15–17] level with the 6-311+G(2d,2p) basis set. At the same level, the MEP are obtained by intrinsic reaction coordinate (IRC) theory with a gradient step-size of 0.03 $(amu)^{1/2}$ bohr. Then, the first and second energy derivatives are obtained to calculate the curvature of the reaction path and the generalized vibrational frequencies along the reaction path. To obtain more accurate energies and barrier heights, the energies are refined by the BMC-CCSD method (a new multi-coefficient correlation method based on the coupled cluster theory with single and double excitations (CCSD) proposed by Lynch and Truhlar) [11] based on the MP2/6-311+G(2d,2p) geometries. Furthermore, the effect of the basis set superposition error on the energies for the reactant precursor complex is considered by means of the counterpoise method proposed by Boys and Bernardi [18]. All electronic structure calculations are performed by GAUSSIAN03 program package [19].

VTST [13,14] is employed to calculate the rate constants by the POLYRATE 9.1 program [12]. The theoretical rate constants for each reaction channel over the temperature range 200–2,000 K are calculated by canonical variational transition states theory (CVT) [14,20] incorporating small-curvature tunneling (SCT) [21,22] contributions proposed by Truhlar and co-workers [14,20]. For the title reactions, all vibrational modes are treated as separable harmonic oscillators, except for the lowest vibrational mode of the three transition states that is treated by the hindered rotor model [23,24]. Note that since there are several methyl groups, have the hindered rotor approximation needs to be applied to the internal rotation of these groups. In order to test the reliability of treating this mode as hindered rotor, we re-estimated the rate constants for R1a by considering the internal rotation of all methyl groups and applying the hindered rotor approximation to reactant, product, and the complex. The detailed results are list in Table S1 as supporting information. By comparing the two results, we found that using the hindered rotor approximation only for one mode and only in the transition state region does not change the rates significantly. Thus, it is reasonable to treat the hindered rotor approximation only for the lowest vibrational mode of the three transition states. The model used for hindered rotor approximation is the torsional mode. Here, we use the RW scheme, where R stands for applying the rectilinear model for calculating the reduced moment of inertia (I_j) of the rotator and the W means using the rotational barrier height (W) from direct ab initio calculation to estimate the vibrational frequency (ω_j). The vibrational frequency can be estimated by $\omega_j = (W_j/2I_j)^{1/2}M$, where M is the total number of minima along the torsional coordinate in the range 0–2π. In this paper, the values of W_j and M are $1,000\,cm^{-1}$ and 9 for R1 and 12 for R2, respectively. In addition, we used "full" approximation level to calculate the partition function. The two electronic states for OH radicals in the calculation of its electronic partition functions, with a $140\,cm^{-1}$ splitting, are considered. The vibrational frequencies along the reaction path are calculated using redundant rectilinear coordinates. Since $SiH(CH_3)_3$ and $Si(CH_3)_4$ are C_{3V} and Td symmetries, respectively, the symmetry factor $\sigma = 1, 9, 12$ for the reaction channels R1a, R1b, and R2 are taken into account in the rate constant calculation. The total rate constants k_1 are calculated from the sum of the individual rate constants, i.e., $k_1 = k_{1a} + k_{1b}$.

3 Results and discussion

3.1 Stationary points

The optimized geometries of the reactants ($SiH(CH_3)_3$, OH and $Si(CH_3)_4$), HBC (CR1aR and CR2P), products ($Si(CH_3)_3$, $SiH(CH_3)_2CH_2$, H_2O, and $Si(CH_3)_3CH_2$) and saddle points (TS1a, TS1b, and TS2) at the MP2/6-311+

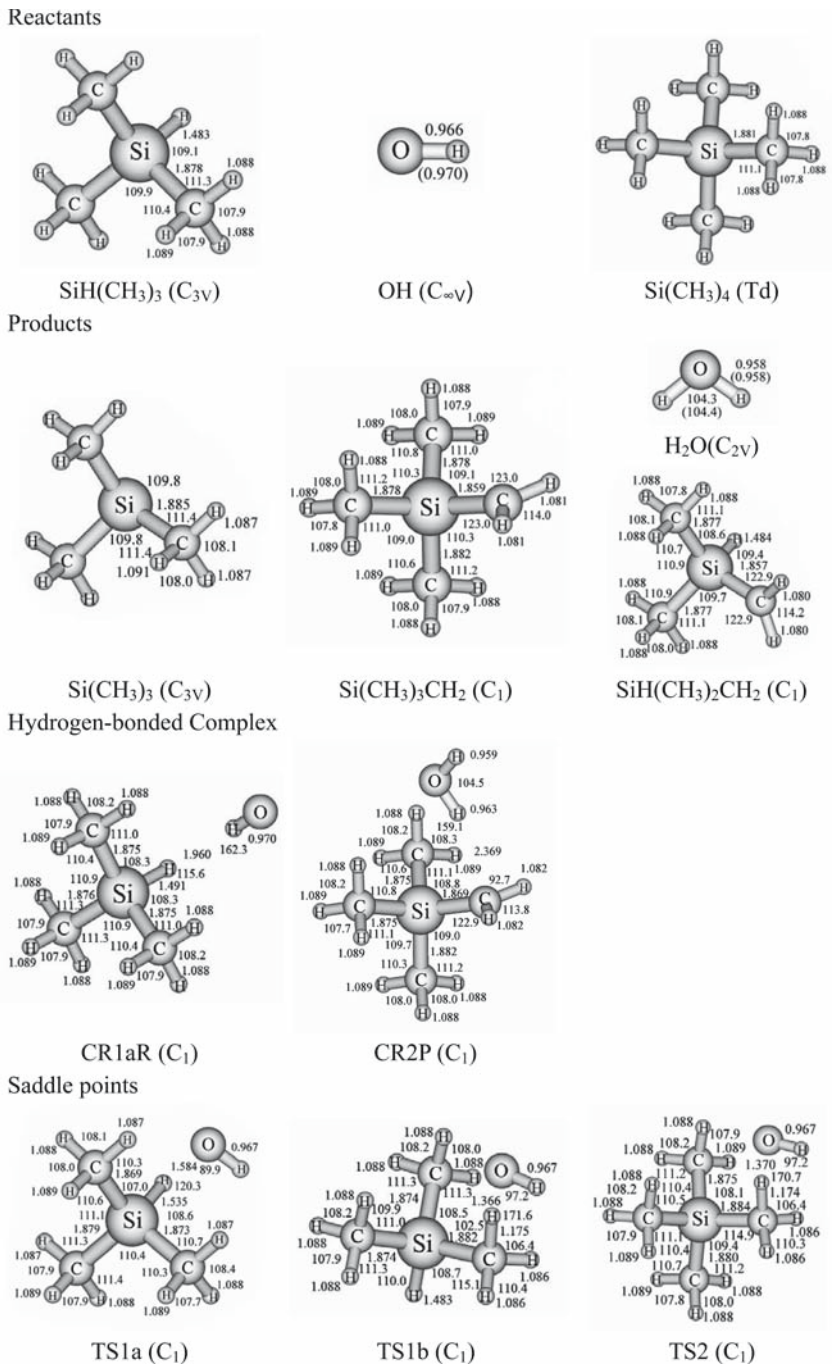

Fig. 1 Optimized geometries of the reactants, products, hydrogen-bonded complexes and saddle points at the MP2/6-311+G(2d,2p) level. The values in *parentheses* are the experimental values (ref [25] for OH, ref [26] for H_2O). Bond length is in angstrom, and angle is in degree

G(2d,2p) level along with the available experimental values [25,26] are presented in Fig. 1. It can be seen that the theoretical geometric parameters of OH and H_2O are in excellent agreement with the corresponding experimental values. And the length of Si–C bond in $Si(CH_3)_4$ is longer than that in $SiH(CH_3)_3$ because of methyl substitution. For the structures of TS1a, TS1b, and TS2, the reactions will proceed via early transition states, consistent with Hammond's postulate [27], applied to for an exothermic hydrogen-abstraction reaction.

The harmonic vibrational frequencies of the reactants, HBC, products, and saddle points calculated at the MP2/6-311+G(2d,2p) level as well as the available experimental values [28–30] as a supplementary information section along to the Cartesian coordinates. For the species OH, $Si(CH_3)_4$, and H_2O, the calculated frequencies are in good agreement with the experimental values with the largest deviation of 6%. The three saddle points are all confirmed by normal-mode analyses to have one and only one imaginary frequency corresponding to the stretching modes of the coupling breaking and forming bonds. And the values of those imaginary frequencies are $728i$ cm^{-1} for TS1a, $1{,}507i$ cm^{-1} for TS1b, and $1{,}465i$ cm^{-1} for TS2.

Table 1 The reaction enthalpies at 298 K (ΔH^0_{298}), the relative energies with and with out zero-point energy (ZPE) correction of hydrogen-bonded complexes (ΔE^c) and TSs (ΔE) (kcal mol^{-1}), and for the reactions of OH radicals with $SiH(CH_3)_3$ and $Si(CH_3)_4$ at the BMC-CCSD//MP2/6-311 + G(2d,2p) level together with the experimental value

		BMC-CCSD//MP2/6-311 + G(2d,2p)	Expt.
ΔH^0_{298}	$OH + SiH(CH_3)_3 \rightarrow Si(CH_3)_3 + H_2O$	−26.31	−24.11 ± 2.63
	$OH + SiH(CH_3)_3 \rightarrow SiH(CH_3)_2CH_2 + H_2O$	−18.75	
	$OH + Si(CH_3)_4 \rightarrow Si(CH_3)_3CH_2 + H_2O$	−18.62	
ΔE	$OH + SiH(CH_3)_3 \rightarrow Si(CH_3)_3 + H_2O$	−2.70	
	$OH + SiH(CH_3)_3 \rightarrow SiH(CH_3)_2CH_2 + H_2O$	2.44	
	$OH + Si(CH_3)_4 \rightarrow Si(CH_3)_3CH_2 + H_2O$	2.00	
ΔE+ZPE	$OH + SiH(CH_3)_3 \rightarrow Si(CH_3)_3 + H_2O$	−2.48	
	$OH + SiH(CH_3)_3 \rightarrow SiH(CH_3)_2CH_2 + H_2O$	0.78	
	$OH + Si(CH_3)_4 \rightarrow Si(CH_3)_3CH_2 + H_2O$	0.35	
ΔE^c + ZPE	$OH + SiH(CH_3)_3 \rightarrow Si(CH_3)_3 + H_2O$	−1.78	
	$OH + Si(CH_3)_4 \rightarrow Si(CH_3)_3CH_2 + H_2O$	−21.33	
ΔE^c	$OH + SiH(CH_3)_3 \rightarrow Si(CH_3)_3 + H_2O$	−2.77	
	$OH + Si(CH_3)_4 \rightarrow Si(CH_3)_3CH_2 + H_2O$	−22.09	

Experimental value derived from the standard heats of formation (in kcal mol^{-1}): $SiH(CH_3)_3$, −39.00 ± 0.96 kcal mol^{-1} [31]; OH, 9.33 kcal mol^{-1} [32]; $Si(CH_3)_3$, 4.07 ± 1.67 kcal mol^{-1} [33]; H_2O, −57.85 kcal mol^{-1} [32]

3.2 Energetics

The reaction enthalpies (ΔH^0_{298}) and the relative energies with and without zero-point energy (ZPE) correction of HBC (ΔE^c) and TSs (ΔE) for the three reaction channels calculated at the BMC-CCSD//MP2/6-311+G(2d,2p) level as well as the available experimental reaction enthalpy are listed in Table 1. It is shown that the three individual reactions are all exothermic reactions, consistent with the discussion above of Hammond's postulate [27]. The theoretical value of ΔH^0_{298} for reaction R1a is −26.31 kcal mol^{-1} which is in good agreement with the corresponding experimental value of −24.11 ± 2.63 kcal mol^{-1} which was derived from the experimental standard heats of formation ($SiH(CH_3)_3$, −39.00 ± 0.96 kcal mol^{-1} [31]; OH, 9.33 kcal mol^{-1} [32]; $Si(CH_3)_3$, 4.07 ± 1.67 kcal mol^{-1} [33]; H_2O, −57.85 kcal mol^{-1} [32]). The reaction enthalpies of reactions R1b and R2 obtained at the BMC-CCSD//MP2 level are −18.75 and −18.62 kcal mol^{-1}, respectively. Due to the lack of the experimental heats of formation for $SiH(CH_3)_2CH_2$ and $Si(CH_3)_3CH_2$ species, it is difficult to make a direct comparison between theory and experiment for the enthalpy of channels R1b and R2. However, in view of the good agreement obtained earlier, it is expected that the enthalpy of reactions R1b and R2 calculated at the same level is reliable.

Note that the energy of reactant is set to zero for reference. For reaction R1a, the complex CR1aR with the relative energy 1.78 kcal mol^{-1} lower than the reactants OH + $SiH(CH_3)_3$ is found at the BMC-CCSD//MP2 level on the reactant side. It is seen that the energy of the complex is very close to the reactants, so one question arises: does the complex really exists or is it an artifact due to the theoretical methods? To test the stability of the complex, the basis set superposition error (BSSE) correction is estimated using the counterpoise method. When the BSSE is considered, the energy of the weakly bonded complex at the MP2/6-311+G(2d,2p) level is 4.13 kcal mol^{-1}. It can be found that the complex CR1aR disappears when BSSE correction is included. For reaction R2, the complex CR2P with the relative energy 2.25 kcal mol^{-1} lower than that of the products at the BMC-CCSD//MP2 level is located at the product side. When BSSE is considered, the energy of the weakly bonded complex is 2.26 kcal mol^{-1} lower than that of the products at the MP2 level, and this means that the weakly bonded complex is existent. The barrier height of reaction R1a taking the value of −2.48 kcal mol^{-1} is about 3.3 kcal mol^{-1} lower than that of the reaction R1b at the BMC-CCSD//MP2/6-311+G(2d,2p) level. At the same time, the former reaction path is more exothermic than the later about 7.55 kcal mol^{-1}, and as a result, the former reaction path is more favorable than the later both thermodynamically and kinetically. If theoretical activation energy (E_a) is estimated based on the calculated CVT/SCT rate constants for reaction channel R1a, the corresponding E_a value is −1.03 kcal mol^{-1} in 200–450 K; this negative activation energy results in the negative temperature dependence.

Table 2 lists the calculated bond dissociation energies (D°_{298}) of the Si–H and C–H bonds in the trimethylsilane, $SiH(CH_3)_3$, along with several experimental data [34–37] of Si–H bond dissociation energy. The D°_{298} (Si–H) value

Table 2 Calculated and experimental bond dissociation energies in $SiH(CH_3)_3$ at 298 K (kcal mol^{-1})

	BMC-CCSD//MP2/6-311+G(2d,2p)	Expt.
D°_{298} (Si–H)	93.28	94.82 ± 0.48[a], 95.06 ± 0.48[b], 95.06 ± 1.43[c], 91.24 ± 1.67[d], 90.28 ± 1.43[e]
D°_{298} (C–H)	100.65	

[a] Ref. [34]
[b] Ref. [35]
[c] Ref. [33]
[d] Ref. [36]
[e] Ref. [37]

with 93.28 kcal mol^{-1}, obtained at the BMC-CCSD//MP2/6-311+G(2d,2p) level, shows good consistency with the previous literature results, 94.82 ± 0.48 [34], 95.06 ± 0.48 [35], 95.06 ± 1.43 [33], 91.24 ± 1.67 [36], and 90.28 ± 1.43 kcal mol^{-1} [37]. At the same level, the D°_{298} (C–H) value in $SiH(CH_3)_3$ is 100.65 kcal mol^{-1}. No comparison between theory and experiment can be made due to the lack of the experimental D°_{298} (C–H) value in $SiH(CH_3)_3$. The above-calculated results show that when the comparison is possible, the agreement between theory and experiment is good. This implies that the BMC-CCSD//MP2/6-311+G(2d,2p) level is a suitable method to compute the bond dissociation energies and our calculated D°_{298} (C–H) value may be expected to provide reliable reference information for future laboratory investigations. The dissociation energy of the Si–H bond is more than 7 kcal mol^{-1} smaller than that of the C–H bond in $SiH(CH_3)_3$, it means that the H-abstraction channel R1a proceeds more effectively than R1b.

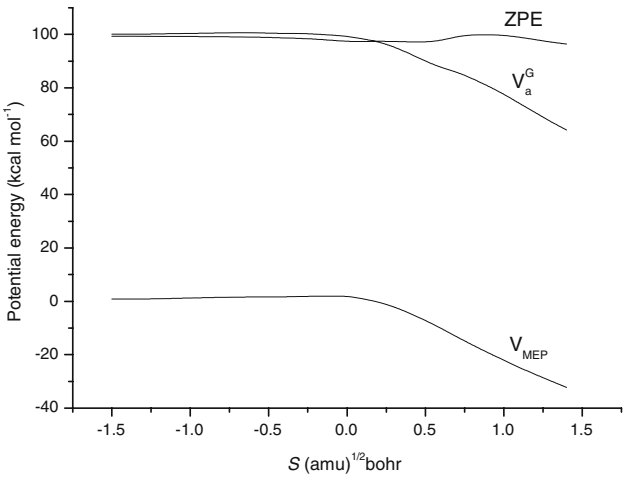

Fig. 2 Classical potential energy curve (V_{MEP}), ground-state vibrationally adiabatic energy curve (V_a^G), and zero-point energy curve (ZPE) as functions of s (amu)$^{1/2}$ bohr at the BMC-CCSD//MP2/6-311+G(2d,2p) level for the reaction $OH + Si(CH_3)_4 \rightarrow Si(CH_3)_3CH_2 + H_2O$

3.3 Rate constants calculation

Dual-level dynamics calculations [7–10] of the title reactions are carried out at the BMC-CCSD//MP2/6-311+G(2d,2p) level. The rate constants of the individual channel are evaluated by canonical transition states theory (TST), canonical variational transition states theory (CVT), and the CVT with the SCT contributions in a wide temperature range from 200 to 2,000 K.

The MEP for reaction R2 is calculated by IRC theory at MP2/6-311+G(2d,2p) level, and the dynamics calculations of the title reaction is carried out with the VTST-ISPE method at the BMC-CCSD//MP2 level. The classical potential energy curve ($V_{MEP}(s)$), the vibrationally adiabatic ground-state potential energy curve ($Va^G(s)$), and the zero-point energy (ZPE) curve of the reaction R2 as a function of the intrinsic reaction coordinate s are plotted in Fig. 2, where $V_a^G(s) = V_{MEP}(s) + ZPE(s)$. As can be seen, the V_{MEP} and V_a^G curves are similar in shape, and the ZPE is practically constant as s varies with only a gentle drop near the saddle point. The same conclusion can be drawn from the other two reaction channels.

The CVT/SCT rate constants of k_{1a} and k_{1b}, the overall CVT/SCT rate constants of k_1, and the TST, CVT, and CVT/SCT rate constants of k_2 together with the experimental values [3–6] are all listed in Table 3. The TST, CVT, and CVT/SCT rate constants of reaction R1a and R1b are plotted against the reciprocal of temperature in Fig. 3, and the overall CVT/SCT rate constants of R1 and R2 as well as the available experimental values [3–6] are displayed against the reciprocal of temperature in Fig. 4. Note that the variational effects, i.e., the ratio between CVT and TST rate constants, are important in the lower temperature range for reaction R1a. The ratios of k_{1a}(CVT)/k_{1a}(TST) are 0.26, 0.54, 0.75, and 0.81 at 200, 400, 800, and 1,500 K, respectively. For reactions R1b and R2, CVT and TST rate constants are nearly the same over the whole temperature range, which indicates that the variational effects are almost negligible. On the other hand, considering the tunneling effect, i.e., the ratio between CVT and CVT/SCT rate constants, for reaction R1a, the CVT and CVT/SCT rate constants are almost the same over the whole temperature range, which means that the tunneling effect is

Table 3 The CVT/SCT rate constants of k_{1a}, k_{1b}, total rate constants k_1 for reaction R1, and TST, CVT, and CVT/SCT rate constants of k_2 for reaction R2 (in cm^3 $molecule^{-1}s^{-1}$) calculated at the BMC-CCSD//MP2/6-311+G(2d,2p) level between 200 and 2,000 K

T(K)	k_{1a}(CVT/SCT)	k_{1b}(CVT/SCT)	k_1(CVT/SCT)	k_{ref}	k_2(TST)	k_2(CVT)	k_2(CVT/SCT)	k_{ref}
200	3.48×10^{-11}	5.63×10^{-14}	3.49×10^{-11}		2.90×10^{-12}	2.90×10^{-12}	2.34×10^{-13}	
225	2.45×10^{-11}	8.82×10^{-14}	2.46×10^{-11}		3.58×10^{-12}	3.57×10^{-12}	3.44×10^{-13}	
250	1.89×10^{-11}	1.23×10^{-13}	1.90×10^{-11}		4.31×10^{-12}	4.28×10^{-12}	4.84×10^{-13}	
296	1.38×10^{-11}	2.19×10^{-13}	1.40×10^{-11}	$(3.1 \pm 0.4) \times 10^{-11}$[a]	5.78×10^{-12}	5.68×10^{-12}	8.26×10^{-13}	$(1.2 \pm 0.2) \times 10^{-12}$[a] $(1.00 \pm 0.27) \times 10^{-12}$[b] $(1.28 \pm 0.46) \times 10^{-12}$[c] $(8.5 \pm 0.9) \times 10^{-13}$[d]
350	1.12×10^{-11}	3.80×10^{-13}	1.16×10^{-11}		7.75×10^{-12}	7.59×10^{-12}	1.37×10^{-12}	
400	1.01×10^{-11}	5.85×10^{-13}	1.07×10^{-11}		9.87×10^{-12}	9.44×10^{-12}	1.87×10^{-12}	
450	9.60×10^{-12}	8.50×10^{-13}	1.05×10^{-11}		1.23×10^{-11}	1.15×10^{-11}	2.55×10^{-12}	
500	9.47×10^{-12}	1.18×10^{-12}	1.07×10^{-11}		1.51×10^{-11}	1.37×10^{-11}	3.36×10^{-12}	
600	9.84×10^{-12}	2.09×10^{-12}	1.19×10^{-11}		2.19×10^{-11}	1.89×10^{-11}	5.43×10^{-12}	
700	1.07×10^{-11}	3.38×10^{-12}	1.41×10^{-11}		3.06×10^{-11}	2.53×10^{-11}	8.21×10^{-12}	
800	1.19×10^{-11}	5.12×10^{-12}	1.70×10^{-11}		4.15×10^{-11}	3.30×10^{-11}	1.18×10^{-11}	
950	1.42×10^{-11}	8.76×10^{-12}	2.30×10^{-11}		6.25×10^{-11}	4.74×10^{-11}	1.90×10^{-11}	
1240	2.01×10^{-11}	2.01×10^{-11}	4.02×10^{-11}		1.22×10^{-10}	8.58×10^{-11}	4.04×10^{-11}	
1500	2.41×10^{-11}	3.64×10^{-11}	6.05×10^{-11}		1.99×10^{-10}	1.31×10^{-10}	6.83×10^{-11}	
2000	2.96×10^{-11}	7.28×10^{-11}	1.02×10^{-10}		4.23×10^{-10}	2.44×10^{-10}	1.33×10^{-10}	

[a] Ref. [3]
[b] Ref. [4]
[c] Ref. [5]
[d] Ref. [6]

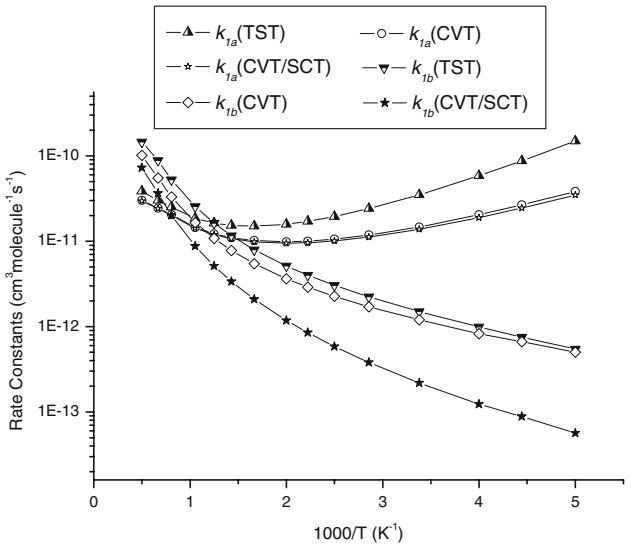

Fig. 3 The TST, CVT and CVT/SCT rate constants of k_{1a} and k_{1b}(cm^3 molecule^{-1}s^{-1}) calculated at the BMC-CCSD//MP2/6-311+G(2d,2p) level for the two reaction channels R1a and R1b versus 1,000/T between 200 and 2,000 K

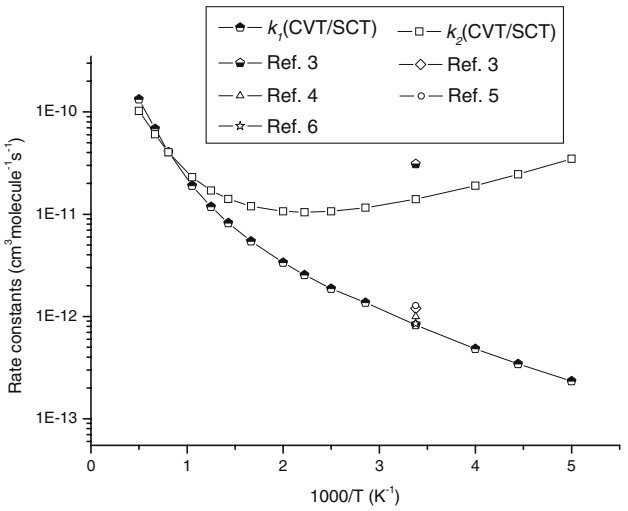

Fig. 4 The CVT/SCT rate constants of k_1 and k_2(cm^3 molecule^{-1}s^{-1}) calculated at the BMC-CCSD//MP2/6-311+G(2d,2p) level for the two reaction R1 and R2 versus 1,000/T between 200 and 2,000 K, together with the experimental value

almost negligible. For reaction R1b and R2, the tunneling effect plays an important role at the lower temperatures. The ratios of k_{1b}(CVT)/k_{1b}(CVT/SCT) are 8.88, 3.86, 2.11, and 1.51 at 200, 400, 800, and 1,500 K, respectively, and the ratios of k_2(CVT)/k_2(CVT/SCT) are 12.4, 5.05, 2.80, and 1.92 at 200, 400, 800, and 1,500 K, respectively. Also, we can find that for reaction R1b and R2, the CVT/SCT rate constants become lower than the CVT ones, which indicates that the quantum effect decreases the rate constant. This is an unusual case of dynamics calculation in which quantum effects preclude particles (supermolecules) to pass over the classical barrier. There are many reactions showing this phenomenon [38–40]. The CVT/CAG and SCT factors for R1-2 are list in Table S2 in the supporting information. We can find that for reaction R1a, the CVT/CAG factors and the SCT factors are close to 1 or equal to 1, while for the reactions R1b and R2, the CVT/CAG factors are small and the SCT factors are 1–2 at lower temperatures. Therefore the CVT/CAG factor is the reason why CVT/SCT is lower than CVT. From Table 3 and Fig. 4, we can easily see that our theoretical CVT/SCT rate constants, k_1 and k_2, are in good agreement with the available experimental values at the measured temperatures, for example, the ratio of k_1(CVT/SCT)/k_1(expt) is 0.45 for R1 at 296 K. For reaction R2, the CVT/SCT rate constants are 0.65–0.97 times of the corresponding experimental results [3–6] at the room temperature. Thus, the present calculation can provide reliable estimations of the rate constants for the title reactions at the higher temperatures.

Figure 3 and Table 3 show that the rate constants of reaction R1a, k_{1a}, are about 1–3 orders of magnitude higher than the ones of reaction R1b, k_{1b}, from 200 to 800 K. Thus, it can be concluded that the H-abstraction channel R1a is always dominant, and reaction R1b is a minor pathway below 800 K. For example, the values of $k_{1a}/(k_{1a} + k_{1b})$ are greater than or equal to 76% in the temperature range 200–500 K. This is consistent with the inferences made from the barrier heights of these two reaction channels. Increasing temperature, the contribution of k_{1b} to the overall rate constant increases gradually, for instance, the ratios $k_{1b}/(k_{1a} + k_{1b})$ are 41% at 800 K, 53% at 1,500 K and 56% at 2,000 K, i.e., the reaction channel R1b becomes more and more competitive. At 1,240 K, the rate constants of R1a and R1b are equal; above that, R1b becomes the major reaction channel. Therefore, the reaction channel R1b should be considered when the temperature increases. The temperature dependence of the branching ratios, $k_{1a}/(k_{1a}+k_{1b})$ and $k_{1b}/(k_{1a}+k_{1b})$, are exhibited against 1,000/T (K^{-1}) in Fig. 5.

As a result of the limited experimental knowledge of the kinetics of the title reaction, we hope that our present study may provide useful information for further laboratory investigations. For convenience of future experimental measurements, the three-parameter fits of the CVT/SCT rate constants of three reaction channels and the whole reaction R1 in the temperature range from 200 to 2,000 K are performed and the expressions are given as follows (in unit of cm^3 molecule^{-1}s^{-1}):

$$k_{1a}(T) = 4.46 \times 10^{-18} T^{2.02} \exp(1,029.43/T)$$
$$k_{1b}(T) = 2.88 \times 10^{-20} T^{2.87} \exp(-141.43/T)$$
$$k_1(T) = 2.53 \times 10^{-21} T^{3.14} \exp(1,352.86/T)$$
$$k_2(T) = 6.00 \times 10^{-19} T^{2.54} \exp(-106.11/T)$$

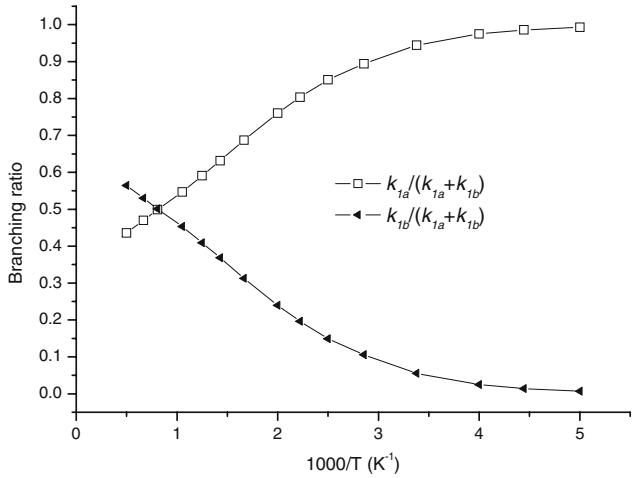

Fig. 5 Calculated branching ratios for the reaction R1 versus 1,000/T between 200 and 2,000 K

4 Conclusion

In this paper, the reactions OH + $SiH(CH_3)_3$ → products, and OH + $Si(CH_3)_4$ → $Si(CH_3)_3CH_2 + H_2O$ are studied by a dual-level direct dynamics method. The potential energy surface information is obtained at the MP2/6-311+G(2d,2p) level, and energies of the stationary points and a few extra points along the MEP are refined at the BMC-CCSD level. For reaction R1, reaction R1a is the major pathway, while the contributions of R1b channel should be considered with the increase in temperature. The rate constants, k_1 and k_2, calculated by CVT incorporating SCT correction at the BMC-CCSD//MP2 level are in good agreement with the available experimental values. The three-parameter rate-temperature formulas for OH + $SiH(CH_3)_3$ and OH + $Si(CH_3)_4$ reactions are fitted and given as follows (in unit of cm^3 $molecule^{-1}s^{-1}$): $k_1(T) = 2.53\times10^{-21}T^{3.14}\exp(1{,}352.86/T)$, $k_2(T) = 6.00\times10^{-19}T^{2.54}\exp(-106.11/T)$. We hope that our results may be useful for further experimental studies on the kinetic properties of the title reactions.

Acknowledgements The authors thank Professor Donald G. Truhlar for providing POLYRATE 9.1 program. This work is supported by the National Natural Science Foundation of China (20333050, 20303007, and 20272011), the Doctor Foundation by the Ministry of Education, the Foundation for University Key Teacher by the Department of Education of Heilongjiang Province (1151G019, 1152G010), and Natural Science Foundation of Heilongjiang Province (TA2005-15, B200605).

References

1. Calvert JG, Atkinson R, Kerr JA, Madronich S, Moortgat GK, Wallington TJ, Yarwood G (2000) The mechanisms of atmospheric oxidation of the alkenes. Oxford, New York
2. Calvert JG, Atkinson R, Becker KH, Kamens RH, Seinfeld JH, Wallington TJ, Yarwood G (2002) The mechanisms of atmospheric oxidation of the aromatic hydrocarbons. Oxford, New York
3. Goumri A, Yuan J, Hommel EL, Marshall P (2003) Chem Phys Lett 375:149
4. Atkinson R (1991) Environ Sci Technol 25:863
5. Sommerlade R, Parlar H, Wrobel D, Kochs P (1993) Environ Sci Technol 27:2435
6. Tuazon EC, Aschmann SM, Atkinson R (2000) Environ Sci Technol 34:1970
7. Truhlar DG (1995) Direct dynamics method for the calculation of reaction rates. In: Heidrich D (ed) The reaction path in chemistry: current approaches and perspectives. Kluwer, Dordrecht, p 229
8. Truhlar DG, Garrett BC, Klippenstein SJ (1996) J Phys Chem 100:12771
9. Hu WP, Truhlar DG (1996) J Am Chem Soc 118:860
10. Corchado JC, Espinosa-Garcia J, Hu W-P, Rossi L, Truhlar DG (1995) J Phys Chem 99:687
11. Lynch BJ, Zhao Y, Truhlar DG (2005) J Phys Chem A 109:1643
12. Corchado JC, Chuang Y-Y, Fast PL, Villa J, Hu W-P, Liu Y-P, Lynch GC, Nguyen KA, Jackels CF, Melissas VS, Lynch BJ, Rossi I, Coitino EL, Ramos AF, Pu J, Albu TV (2002) POLYRATE version 9.1. Department of Chemistry and Supercomputer Institute. University of Minnesota, Minneapolis
13. Truhlar DG, Garrett BC (1980) Acc Chem Res 13:440
14. Truhlar DG, Isaacson AD, Garrett BC (1985). In: Baer M (eds) The theory of chemical reaction dynamics, vol 4, CRC P, Boca Raton, p. 65
15. Duncan WT, Truong TN (1995) J Chem Phys 103:9642
16. Frisch MJ, Head-Gordon M, Pople JA (1990) Chem Phys Lett 166:275
17. Head-Gordon M, Pople JA, Frisch MJ (1988) Chem Phys Lett 153:503
18. Boys SF, Bernardi F (1970) Mol Phys 19:553
19. Frisch MJ, Trucks GW, Schlegel HB, Scuseria GE, Robb MA, Cheeseman JR, Montgomery JA, Jr, Vreven T, Kudin KN, Burant JC, Millam JM, Iyengar SS, Tomasi J, Barone V, Mennucci B, Cossi M, Scalmani G, Rega N, Petersson GA, Nakatsuji H, Hada M, Ehara M, Toyota K, Fukuda R, Hasegawa J, Ishida M, Nakajima T, Honda Y, Kitao O, Nakai H, Klene M, Li X, Knox JE, Hratchian HP, Cross JB, Adamo C, Jaramillo J, Gomperts R, Stratmann RE, Yazyev O, Austin AJ, Cammi R, Pomelli C, Ochterski JW, Ayala PY, Morokuma K, Voth GA, Salvador P, Dannenberg JJ, Zakrzewski VG, Dapprich S, Daniels AD, Strain MC, Farkas O, Malick DK, Rabuck AD, Raghavachari K, Foresman JB, Ortiz JV, Cui Q, Baboul AG, Clifford S, Cioslowski J, Stefanov BB, Liu G, Liashenko A, Piskorz P, Komaromi I, Martin RL, Fox DJ, Keith T, Al-Laham MA, Peng CY, Nanayakkara A, Challacombe M, Gill PMW, Johnson B, Chen W, Wong MW, Gonzalez C, Pople JA (2003) Gaussian 03, Gaussian, Inc. , Pittsburgh
20. Steckler R, Hu W-P, Liu Y-P, Lynch GC, Garrett BC, Isaacson AD, Melissas VS, Lu D-P, Troung TN, Rai SN, Hancock GC, Lauderdale JG, Joseph T, Truhlar DG (1995) Comput Phys Commun 88:341
21. Lu DH, Truong TN, Melissas VS, Lynch GC, Liu YP, Grarrett BC, Steckler R, Issacson AD, Rai SN, Hancock GC, Lauderdale JG, Joseph T, Truhlar DG (1992) Comput Phys Commun 71:235
22. Liu Y-P, Lynch GC, Truong TN, Lu D-H, Truhlar DG, Garrett BC (1993) J Am Chem Soc 115:2408
23. Truhlar DG (1991) J Comput Chem 12:266
24. Chuang YY, Truhlar DG (2000) J Chem Phys 112:1221
25. Huber KP, Herzberg G (2005) NIST chemistry webbook, nist standard reference database number 69, June 2005 release constants of diatomic molecules date
26. Kuchitsu K (1998) In: Structure of free polyatomic molecules basic data. Springer, Berlin, p 58
27. Hammond GS (1955) J Am Chem Soc 77:334

28. Shimanouchi T (1972) Tables of molecular vibrational frequencies consolidated volume I. National Bureau of Standards, US GPO, Washington, DC
29. Coblentz Society, Inc (2005) NIST chemistry webbook, NIST standard reference database number 69, June 2005 release, Vibrational frequency date
30. Shimanouchi T (2005) NIST chemistry webbook, NIST standard reference database number 69, June 2005 release, Vibrational frequency date
31. Walsh R (1992) In: Martinho Simões JA (eds) Energetica of organometallic species; NATO-ASI series C, 367 Kluwer, Dordrecht Chapter 11
32. Chase MW, Jr (1998) NIST-JANAF themochemical tables, 4th edn. J Phys Chem Ref Data Monogr 9: 1–1951
33. Ding L, Marshall P (1992) J Am Chem Soc 114:5754
34. Kalinovski IJ, Gutman D, Krasnoperov LN, Goumri A, Yuan W-J, Marshall P (1994) J Phys Chem 98:9551
35. Goumri A, Yuan W-J, Marshall P (1993) J Am Chem Soc 115:2539
36. Ellul R, Potzinger P, Reimann B, Camilleri P (1981) Ber Bunsen-Ges Phys Chem 85:407
37. Doncaster AM, Walsh R (1979) J Chem Soc, Faraday Trans 1(75):1126
38. Zhang QZ, Wang SK, Gu YS (2002) J Phys Chem A 106:3796
39. Taghikhani M, Parsafar GA (2005) J Phys Chem A 109:8158
40. Ji YM, Wang L, Li ZS, Liu JY, Sun CC (2006) Chem Phys Chem 7:1741